Journal Name

ARTICLE

Open and closed forms of the interpenetrated $[Cu_2(Tae)(Bpa)_2](NO_3)_2{\cdot}nH_2O$ cationic coordination polymer: magnetic properties and high pressure CO_2/CH_4 gas sorption.

Received 00th January 20xx,
Accepted 00th January 20xx

DOI: 10.1039/x0xx00000x

www.rsc.org/

Roberto Fernández de Luis,[a] Edurne S. Larrea, [b] Joseba Orive,[c] Arkaitz Fidalgo-Marijuan,[a] Luis Lezama,[a,d] María I. Arriortua.[a,b]

Two closed and one open structural forms of the interpenetrated $[Cu_2(Tae)(Bpa)_2](NO_3)_2{\cdot}nH_2O$ (H_2Tae= 1,1,2,2-tetraacetylethane, Bpa= 1,2-Bis(4-pyridyl)ethane) cationic coordination polymer have been synthesized. Three crystallographically related interpenetrated *"ths"* cationic nets encapsulate water molecules and nitrate anions giving rise to the closed structural forms of $[Cu_2(Tae)(Bpa)_2](NO_3)_2{\cdot}nH_2O$. Depending on the location of water molecules and nitrate groups, two different closed forms, with 5.5 and 3.6 crystallization water molecules have been obtained. Thermal activation of the closed structures gives rise to a 29% expansion of the unit cell. This closed to open transformation is reversible, and is triggered by the loss or uptake of solvent. The high pressure gas adsorption experiments show similar selectivity values towards CO_2 for CO_2/CH_4 mixtures than that showed by some metal organic frameworks without unsaturated metal sites, and isosteric heats for CO_2 adsorption similar to that for the HKUST-1 compound.

Introduction

Design of new porous metal organic coordination polymers constructed from pre and post synthetic tuneable metal nodes and organic linkers is currently one of the most active research fields in materials science. [1] Just to mention some examples, gas storage, [3] molecular magnetism, [4] molecular recognition and sensing, [5] thermal dynamic response, [6] protonic conductivity, [7] pollutants capture, [8] catalysis [9] or photovoltaic and photo-catalysis [10] are current research areas where the coordination porous polymers are applied.

Based on the principles of reticular chemistry, a broad spectrum of structural architectures constructed from carboxylate, imidazole, tetrazolate, phosphonate and/or pyridine organic linkers combined with metal centres or clusters have been synthesized during the last decade [11], but the coordination chemistry of metal β-diketonate clusters as starting building units for the design of extended porous frameworks is still a very poorly explored approach.

Initially, several low dimensional dimeric, triangular and rectangular molecular cages and boxes linked through weak interactions (hydrogen bonding, Van der Walls, π···π interactions) were obtained based on diketonate functionalized benzene and naphthalene ligands [12-17], but there are very scarce examples of extended frameworks constructed from metal-diketonate motifs.

The first three dimensional porous metal-diketonate polymer based on metal- Tae (H_2Tae: 1,1,2,2-tetraacetylethane) motifs were reported by Q. Yang *et. al.* [18] The fast deprotonation of H_2Tae ligand in the synthesis media compensates the positive charge of the metal cations giving rise to a fast precipitation of the metal-diketonate particles, generating a low crystalline M-Tae hydrogels. The authors suggest possible extended structures of M(II)Tae and M(III)Tae compounds, but the low crystallinity and small particle size of M-Tae compounds hinder the determination of a reliable structural model. [18]

In order to reduce the fast precipitation of Metal-Tae based compounds, the H_2Tae and metal cations can be combined with neutral pyridine-based ligands to generate crystal architectures similar to these obtained by the combination of carboxylate and pyridine linkers. The main studies exploring this approach have been focused on the combination of Tae with chelating molecules, such as 2,2´-bipyridine, 1,10-phenanthroline or di-2-pyridylamine. [19] Indeed, as far as we know, only two extended architectures based on Metal-Tae-

[a] *BCMaterials (Basque Center for Materials, Applications & Nanostructures),Technological Park of Zamudio, Camino de Ibaizabal, Bndg. 500-1st, 48160, Derio, Spain.*
[b] *Departamento de Mineralogía y Petrología, Facultad de Ciencia y Tecnología, Universidad del País Vasco, UPV/EHU. 48940, Leioa, Spain.*
[c] *Departamento de Ciencia de Materiales, Facultad de Ciencias Físicas y Matemáticas (FCFM), Universidad de Chile. Av. Beauchef 851, Santiago, Chile*
[d] *Departamento de Química Inorgánica, Facultad de Ciencia y Tecnología, Universidad del País Vasco, UPV/EHU. 48940, Leioa, Spain.*

† Footnotes relating to the title and/or authors should appear here.

Electronic Supplementary Information (ESI) available: [**Tables S1** Bond distances and angles for Closed·$5H_2O$ and Closed·$3.6H_2O$. **Fig. S.1.-** Distortion maps **Fig. S.2.-** Thermogravimentric/DSC curves, **Fig. S.3.-** Thermodiffractometry of Closed·$5H_2O$. **Fig. S.4.-** Reversibility of Closed-Open transformation. **Fig. S.5.-** Solid reflectance spectra.**Fig. S.6.-** Thermodiffractometry of Open·$2.4H_2O$.**Fig. S.7.-** Thermal evolution of the cell parameter and cell volume for Open·$2.4H_2O$. **Fig. S.8.-** Magnetic susceptibility measurements. **Fig. S.9.-**N_2 adsorption isotherm at 77K/IAST CO_2/CH_4 selectivity. **Fig. S.10.-** Van Hoff Plot for (a) CO_2 y (b) CH_4. **Fig. S.11.**-Simulated and experimental X-ray diffraction patterns]. See DOI: 10.1039/x0xx00000x

pyridine combination have been reported: the commensurate modulated $[Cu(H_2O)(HTae)(4,4´\text{-}Bpy)](NO_3)$ one dimensional structure studied by Fernández de Luis *et al.* [20] and the three $[Cu_2(Tae)(4,4´\text{-}Bpy)_2]$ $[(NO_3)_2]^2$ concomitant supramolecular isomers synthesized by Luisi *et al*. [21]

Giving a step forward, we have explored the crystal chemistry of the Cu-Tae-Bpa (1,2-Bis(4-pyridyl)ethane) system, obtaining the interpenetrated $[Cu_2(Tae)(Bpa)_2](NO_3)_2{\cdot}nH_2O$ three-dimensional framework. As in many other systems explored before, the increase of the length of the organic ligand induces a crystallization of interpenetrated metal-organic nets, limiting the porous accessible volume of the crystal structure. [22] Nevertheless, the interpenetration may confer exotic dynamic responses to the crystal framework against external stimuli [23], such as solvent loss/replacement or gas adsorption, which can induce a net-opening structural transformation at a critical pressure or guest uptake. [24] Examples of closed (narrow pore crystal structure) and open (open pore crystal structure) transformations have been reported both for non-interpenetrated and interpenetrated frameworks, being the interactions established by the metal organic scaffold and the encapsulated molecules critical to stabilize the closed form. It is worthy to mention that the breathing mechanisms are different in interpenetrated and non-interpenetrated frameworks. While in non-interpenetrated structures, the structural response is driven by the cooperative arrangement of the structural building blocks (metal clusters and linkers), in interpenetrated coordination polymers, the net-opening happens mainly through the displacements of the interpenetrated nets.

Herein, we report the crystal structures of two closed forms of $[Cu_2(Tae)(Bpa)_2](NO_3)_2{\cdot}nH_2O$ (n=5.5 and 3.6, hereafter Closed·$5H_2O$ and Closed·$3.6H_2O$, respectively) and the qualitative structural model for the open hydrated and anhydrous forms ($[Cu_2(Tae)(Bpa)_2](NO_3)_2.nH_2O$ (n=2.4 and n=0, hereafter Open·$2.4H_2O$ and Open·An, respectively)) of a new cationic coordination polymer. The thermogravimetric and thermodiffractometric studies allow proposing the transformation mechanism involved in the closed to open structural transformation. This dynamic response has been followed by FT-IR, EPR and UV-visible diffuse reflectance spectroscopies. Magnetic properties have been studied and compared with the previously reported study for the one dimensional $[Cu(H_2O)(HTae)(4,4´\text{-}Bpy)](NO_3)$ coordination polymer reported by Fernández de Luis *et al.* [20]. Finally, the high pressure CO_2 and CH_4 adsorption studies have demonstrated that the insertion of gas molecules within the structure is boosted by the flexibility of the interpenetrated nets, even when the initial surface area of the studied compound is low.

Crystal structure of Closed forms

The crystal structures of Closed·$5H_2O$ and Closed·$3.6H_2O$ phases have been determined by single crystal X-ray diffraction. The asymmetric units for Closed·$5H_2O$ and Closed·$3.6H_2O$ are depicted in Figs. 1 (a) and (b), respectively. Both contain a half of Bpa and Tae molecules and one copper atom located at a 16f Wyckoff special position.

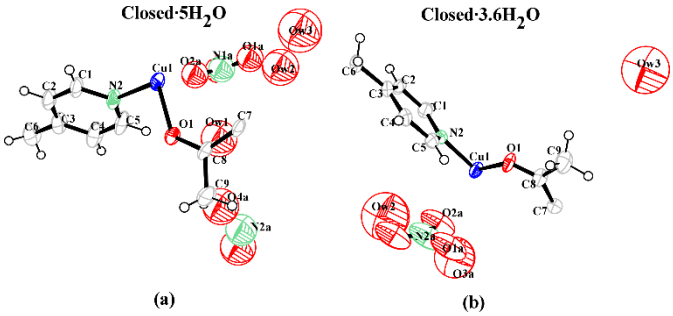

Fig. 1. Asymmetric units of (a) Closed $5H_2O$ and (b) Closed $3.6H_2O$ compounds.

For Closed·$5H_2O$, the nitrate group is disordered in two positions with occupancy factors of 0.25. One of the disordered nitrate groups is semi-coordinated to the copper atoms while the second anion is located within the pores of the crystal structure. Finally, there are three crystallographically independent disordered crystallization water molecules with 0.5 (Ow1), 0.4 (Ow2) and 0.35 (Ow3) occupancy factors. For Closed·$3.6H_2O$, there is only one crystallographic independent nitrate group with a 0.5 occupancy factor, which is semi-coordinated to the copper cation. The crystallization water molecules are located in three different crystallographic sites with 0.5 (Ow1), 0.3 (Ow2) and

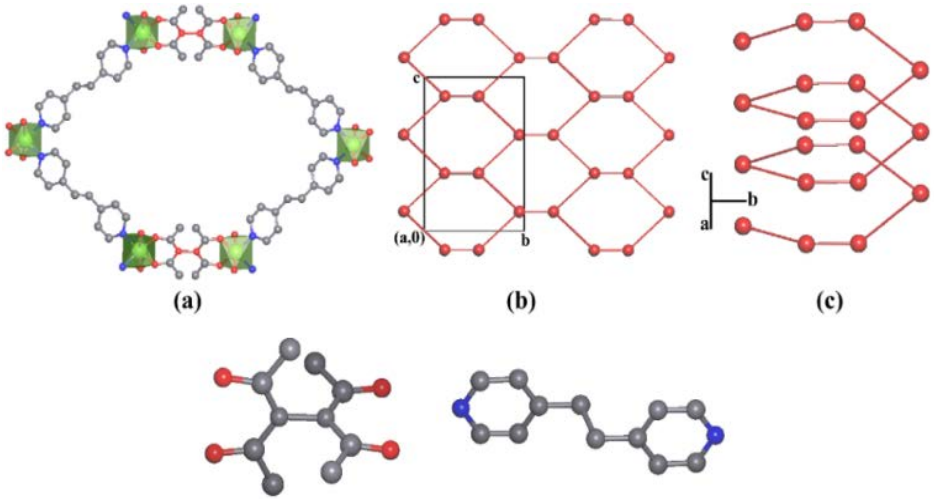

Fig. 2 (a) Connectivity between the copper metal centers (green polyhedra) through Bpa and Tae organic ligands. (b) Simplification of the $[Cu_2(Tae)(Bpa)_2]^+$ crystal framework *("ths"* topology) (c) Cu-Bpy-Cu-Bpy-Cu-Tae-Cu helical metal organic chains within the three dimensional *"ths"* net. (d) Tae (1,1,2,2-tetraacetylethane) organic ligand. (e) Bpa (1,2-Bis(4-pyridyl)ethane) organic ligand. Hydrogen atoms have been omitted for clarity.

0.25 (Ow3) occupancy factors.

For both crystal structures, each copper cation is connected to other three symmetry related metal centres through two Bpa and one Tae organic ligands. The linkage between copper cations through organic linkers generates a 3D 3-connected net with $10^2 \cdot 10^4 \cdot 10^4$ vertex symbol and *"ths"* type topology. Fig. 2 depicts the connectivity between the copper metal centres through the organic ligands (Fig. 2 (a)) and the simplified *"ths"* topology considering the copper cations as the nodes, and the organic molecules as the linkers (Fig. 2(b)). Each hexagonal pore of a single *"ths"* net is formed by Cu-Bpy-Cu-Tae helical metal organic springs oriented along the [100] crystallographic direction (Fig. 2(c)).

The crystal structure of both compounds contains three *"ths"* interpenetrated nets (class Ia) with full interpenetration vectors FIV= [1/2, 1/2, 0] and [1/2, -1/2, 0]. The FIV vectors are directly related to the translational symmetry of F centred Bravais lattice, of the *Fddd* space group (Fig. 3).

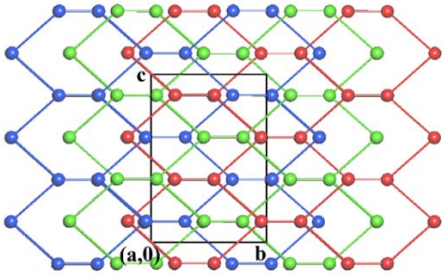

Fig. 3. Simplified interpenetrated "ths" metal organic nets in Closed·$5H_2O$.

Despite the interpenetrated frameworks of Closed·$5H_2O$ and Closed·$3.6H_2O$ compounds are very similar; the location of the nitrate groups and crystallization water molecules within the anions are trapped. The pores are depicted in Figure 4 and will be denoted here and after as A and B pores. In order to visualize better the volume occupied by the water molecules in the crystal structures, the Voronoi-Dirichlet polyhedra (VDP) of the Ow1, Ow2 and Ow3 oxygen atoms have been constructed (red polyhedra in Fig. 4).

The main difference between Closed·$5H_2O$ and Closed·$3.6H_2O$ lies in the position and role of the nitrate groups. In Closed·$5H_2O$ two types of nitrates groups are found. The first type of nitrate anion is disordered in two positions and located within the pores of the interpenetrated crystal framework (nitrate groups represented with a yellow colour in Fig. 4 (a.2) and (a.3)). The second type of nitrate molecules are forming part of the pseudo-coordination sphere of the copper cations ($Cu\text{-}O_{Nitrate}$) (nitrate groups represented with a blue colour in Fig. 4 (a.2) and (a.3)). In Closed·$3.6{\cdot}H_2O$, both in the A and B pores (Fig. 4 (b.1)), all the nitrate groups are disordered in two different positions with a 0.5 occupancy factor and forming part of the pseudo-coordination environment of the copper(II) cations (nitrate groups represented with a blue colour in Fig. 4 (b.2) and (b.3)).

These differences between the solvent and anion distribution within the pores of the Closed·$5H_2O$ and Closed·$3.6H_2O$ crystal structures give rise to slight differences in the cell parameters, and hence in the interpenetration distances between the *"ths"* nets.

Table S1 summarizes the selected bond distances and angles for Closed·$5H_2O$ and Closed·$3.6H_2O$. The coordination environment of the copper atoms can be described as an axially elongated octahedron. Due to the occupancy factor of the nitrate anions, the axial positions of the octahedron are randomly occupied at 25% in Closed·$5H_2O$ and at 50% in Closed·$3.6H_2O$. Given the average picture of the crystal

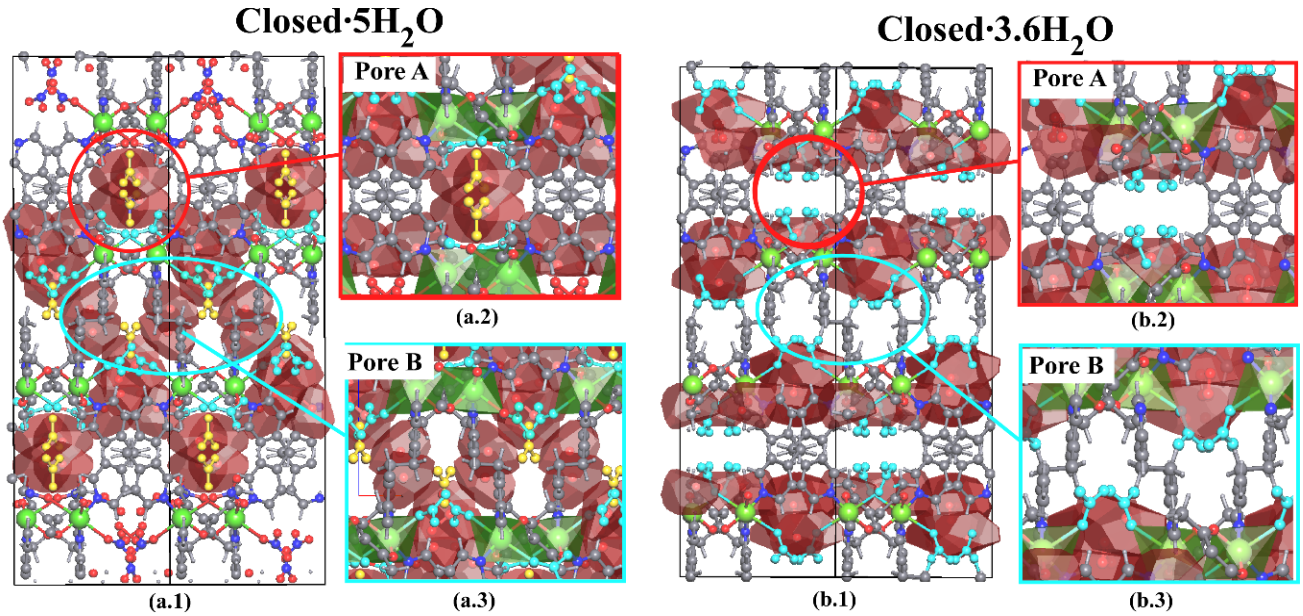

Fig. 4: (a.1)-(b.1) Pictures of the Pores A and B of Closed·$5H_2O$ and Closed·$3.6H_2O$ crystal structure. (a.2)-(b.2) Details of the Pores A of Closed·$5H_2O$ and Closed·$3.6H_2O$. (a.3)-(b.3) Detailed picture of the Pores B of Closed·$5H_2O$ and Closed·$3.6H_2O$. Uncoordinated nitrate groups: yellow colored. Semi coordinated nitrate anions: blue colored. Voronoi-Dirichlet polyhedra of water molecules: red colored polyhedra.

pores differs. The interpenetration of the nets generates two different pores in which the water molecules and nitrate

structures obtained from the X-ray diffraction data, it is not possible to discern the different local environment of the

copper cations. Thus, considering the nitrate occupation factors, octahedral, five coordinated square pyramidal and square planar local coordination environments are possible for the copper cations. The equatorial plane of the six-coordinated copper cations contains two oxygen and two nitrogen atoms belonging to one HTae and two Bpa organic molecules. The axial positions of the octahedra are occupied by nitrate groups. The Cu-O_{Tae} bond distances are the shortest ones, with values of 1.898(4) Å and 1.911(5) Å for Cu1-O1 in Closed·5H_2O and Closed·3.6H_2O, respectively. The Cu-N_{Bpy} bonds are slightly longer with distance values of 2.004(5) Å and 1.984(6) Å for Cu1-N2 in Closed·5H_2O and Closed·3.6H_2O structures, respectively. The axially elongated Cu-$O_{Nitrate}$ bonds take distances of 2.504(8) Å (Closed·5H_2O) and 2.629(9) Å (Closed·3.6H_2O). The later inter-atomic distances are appreciably longer than the bond lengths in the equatorial positions of the copper octahedra, but within the range of weak covalent interactions termed "pseudo-coordination".[25] The *trans* and *cis* angles of the copper octahedron are near to the ideal values of 90º and 180º of a regular octahedron. Continuous shape measurements of the metal coordination environments were carried out with Shape v2.1 program, [26] considering octahedral and square planar coordination environments. For both closed compounds, the octahedral environment are near the ideal geometry, but with the coordination sphere exhibiting an elongation because of the Jahn-Teller effect. Considering a four-coordination sphere, the square planar geometry exhibits a considerable spread deformation towards a tetrahedral geometry (Fig. S1).

Regarding the C-C and C-O bond distances of the HTae ligand, two type of bond lengths are found. The first ones associated to the C-C single bonds (ca. 1.49 Å) involving the methyl groups, and the second ones to the resonant C=C (ca. 1.40 Å) and C=O (ca. 1.30 Å) bonds.

The bond valence calculations have been carried out considering only the equatorial atoms of the octahedral environment. The calculations confirm the 2+ valence of the copper cations and the negligible contribution of the nitrate anions (Table 1). [27]

Table 1 Bond valence parameters calculated for copper cations in Closed·5H_2O and Closed·3.6H_2O forms (BVS: Bond valence sum).

Closed 5H_2O		
Cu1-N2 x 2	2.0044	0.504 x2= 1.008
Cu1-O1 x2	1.8980	0.553 x2= 1.106
BVS		2.114
Closed 3.6H_2O		
Cu1-N2 x 2	1.9839	0.533 x 2= 1.066
Cu1-O1 x2	1.9114	0.534 x 2= 1.068
BVS		2.134

Crystal structure of Open forms

The low crystallinity and small size of the single crystals of Open·2.4H_2O compound hinder the construction of any reliable structural model from single crystal or powder X-ray diffraction data. Given the complexity of the closed forms crystal structures and the crystallinity of the X-ray diffraction patterns there is not enough information to carry out a Rietveld refinement starting from the structural models of the closed compounds.

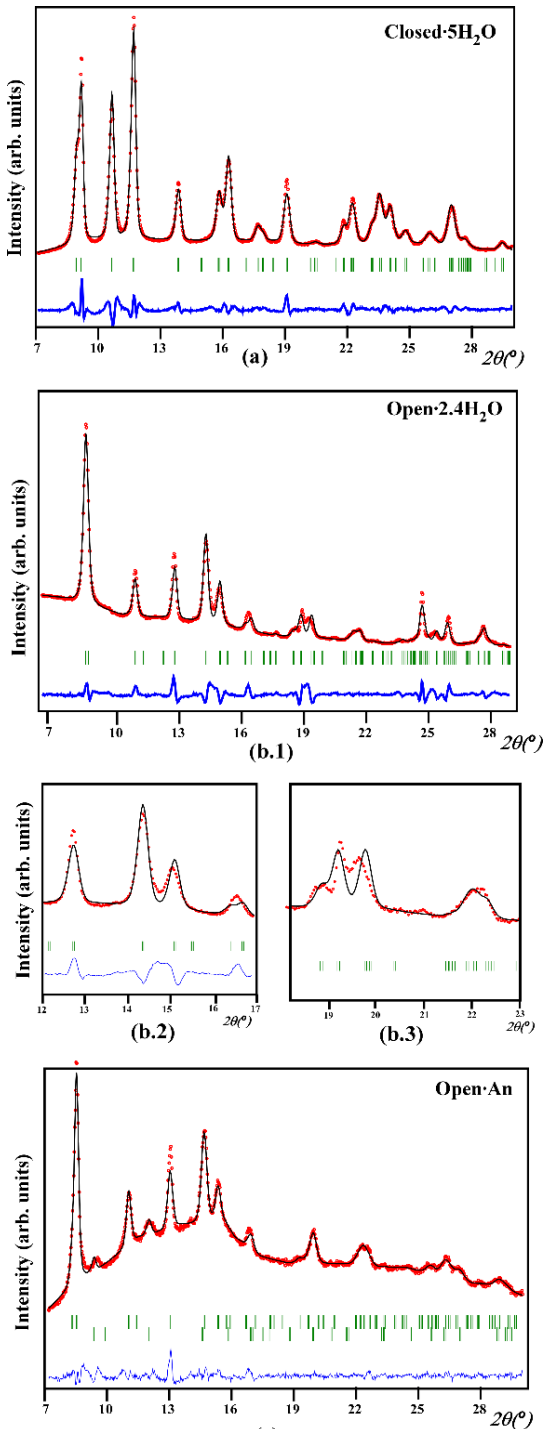

Fig. 5 Pattern matching analyses for (a) Closed·5H_2O and (b.1) Open·2.4H_2O as synthesized samples. The *Fddd* space group was used for the fittings. (b.2)-(b.3) Detailed picture of some mismatches between the *Fddd* model and the experimental data between 12 and 23º in 2θ (º). (c) Pattern matching analysis of the thermally activated Open·An sample. Small presence of Closed·5H_2O phase is observed in the preparation due to the uptake of water of the sample from environmental moisture.

Nevertheless, qualitative structural model for open forms can be suggested based on the similitudes between the powder patterns of the closed and open compounds. The powder X-ray diffraction pattern of Open·2.4H_2O is similar to this one of the Closed·5H_2O structure, but some of the most intense diffraction maxima show a strong displacement to lower *2ϑ(º)* values, and hence, the cell parameters related with these crystallographic spacing are expected to be larger than the cell parameters of the closed structures. Starting from the cell parameters and symmetry (S.G. *Fddd*) obtained from single crystal data of Closed·5H_2O, the profile matching of the same compound (Fig. 5(a)) and of the Open·2.4H_2O pattern were carried out (Fig. 5 (b)). Despite a reasonable fit is obtained for the low *2ϑ* angle reflections, there are clear mismatches at high angles that cannot be solved with an *Fddd* orthorhombic symmetry (Fig. 5 (b.2-b.3)). In a second attempt, pattern-matching analyses were also carried out with the lower symmetry *Fdd2*, *F222* and *C2/c* subgroups of *Fddd* space group, without success. To accomplish a proper fit of high *2ϑ* angle reflections, there is a need to break the symmetry of the F cell. The reduction of the symmetry to a P cell gives rise to a good fit of the high angle reflections, but due to the high overlapping of the reflection positions, the obtained crystal parameters have to be interpreted carefully. Any reduction of the F lattice symmetry involves the generation of different independent copper, Tae and Bpa crystallographic positions in the structures. Depending on the selected symmetry, two effects could be observed after the structural transformation: i) the generation of crystallographic independent *"ths"* nets, and/or ii) the distortion of the *"ths"* individual nets.

Assuming this small deviation from the F high symmetry closed structural model, it is preferable to consider the *Fddd* space group to obtain more accurate cell parameters and volume from the individual fits of the (004), (040) and (133) reflections. The comparison between the crystallographic cells obtained for Closed·5H_2O and Open·2.4H_2O compounds indicates a 9.7% and 22.8% increase of the "a" and "b" parameters from the closed to the open form, respectively. As a result, the cell volume increases a 29%. (Table 2).

Table 2 Cell parameters and volume obtained from the pattern matching analysis of Closed·5H_2O and peak fit of the (040), (400) and (113) maxima of Open·2.4H_2O compounds.

	a (Å)	b (Å)	c (Å)	Vol (Å^3)
Closed·5H_2O	11.591(3)	22.730(7)	33.05(1)	9092(5)
Open·2.4H_2O	12.715(5)	27.920(6)	33.073(8)	11741(2)
Diff. (%)	9.7	28	0	29

Assuming that the *"ths"* interpenetrated framework is stable after the closed to open transformation, the 22.8% of increase in the "b" parameter can be explained based on the separation of *"ths"* nets along the [010] crystallographic direction (Scheme 1 (a)). Simultaneously, the Cu-Tae-Cu-Bpy helical chains can act as a metal organic spring, stretching along the [100] direction, and giving rise to the 9.7% increase in the "a" parameter (Scheme 1 (b)).

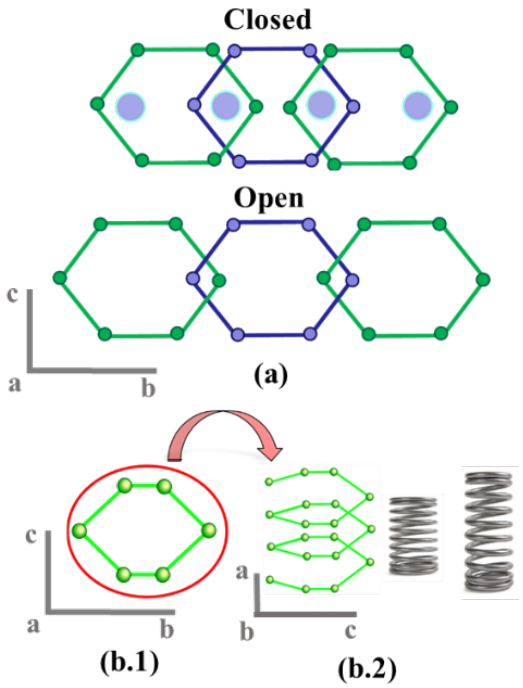

Scheme 1. a) Simplified model of closed to open structural transformation due to the loss of guest molecules. (b.1)-(b.2) One of the metal organic springs within the *"ths"* network. Mechanism involving the increase of the "a" parameter due to the stretching of the metal organic springs.

Thermal properties

The thermal, spectroscopic and magnetic properties have been studied only for Closed·5H_2O and Open·2.4H_2O compounds, because Closed·3.6H_2O is solely obtained as a minor crystallization by-product. Thermogravimetric analyses of Closed·5H_2O and Open·2.4H_2O phases are very similar, as expected taking into account the similarities of their crystal structures (Fig. S2). There are three different weight losses: i) The first one occurs near room temperature and is associated to the release of crystallization water molecules encapsulated within the pores of the crystal structures (Closed·5H_2O: 40ºC-90ºC exp: 9.44%, theor. 9.93%, Open·2.4H_2O: 30-60ºC exp: 4.90%, theor. 5.03%), ii) The second and third steps involve the nitrate groups release and organic ligands calcination. The process starts at 120 ºC for both compounds ending at 290ºC for Closed·5H_2O (exp: 72.24%, theor. 73.66 %) and 340ºC for Open·2.4H_2O (exp: 80.12%, theor. 80.18%).

Thermodiffractometric analysis of Closed·5H_2O structure reveals that the closed to open form transformation occurs at 60ºC (Fig. S3). In comparison with Closed·5H_2O, the powder patterns of the thermally activated Open·An phase show an acute loss of crystallinity, which indicates that the long-range order is partially loss during the transformation (Fig. 5 (c)).

Such open-closed transformation is a reversible process triggered by the direct addition of water to the open compound. Indeed, the structural change can be induced by the inclusion of different solvents, such as methanol, ethanol, propanol or tetrahydrofuran (Fig. S4). [28] It is worthy to

mention that the loss of crystallinity after the thermal activation of Closed form samples is not recovered after the inclusion of solvents.

No differences in the IR spectra of Closed·5H_2O and thermally activated open form are appreciated, which indicates the structural stability of the basic building blocks after the transformation.

Diffuse reflectance UV-Vis spectra of Closed·5H_2O and Open·An (Fig. S5) show that the coordination environment of the copper cations is slightly affected during the transformation. UV-Vis spectra present broad bands centred at 660 nm (Closed·5H_2O) and 627 nm (Open·An). These bands are in good agreement with the "d-d" transition of the Cu(II) cation in an octahedral environment, and their broadness is characteristic of a single octahedral copper (II) complex, as a consequence of the Jahn-Teller effect.

Thermodiffactometric analysis of the as-synthesized Open·2.4H_2O compound was also carried out (Fig. S6). In comparison with Closed·5H_2O, Open·2.4H_2O does not show any sudden structural transformation due to the loss of guest molecules, and a continuous structural compression associated to the loss of crystallization water molecules is observed between 30 and 60ºC (Fig. S7). After the release of the solvent, the thermal expansion of the crystal structure takes place mainly through the increase of the "a" parameter. [29]

Electron paramagnetic spectroscopy

The EPR spectra of the Closed·5H_2O and Open·2.4H_2O compounds are practically equivalents, so for sake of simplicity only the spectra for Closed·5H_2O and Open·An compounds have been plotted in Fig. 6.

The Q-band EPR spectrum of Closed·5H_2O shows the characteristic shape of Cu(II) chromophores with rhombic symmetry. No hyperfine structure is observed (Fig.6). The best fitting g-vales obtained are g_1 = 2.198, g_2 = 2.130 and g_3 = 2.063 (g_{iso}= 2.130). The main g-values are remaining practically unchanged from room temperature down to 5 K. The calculated G parameter is 2.05, which indicates that the g values obtained from experiment are not equal to the molecular ones and do not reflect the individual geometries of our copper chromospheres. The rhombic X-band spectra of Closed·5H_2O compound is not well defined, and can be described as a quasi-isotropic signal with a main value for g= 2.132. Taking into account our previous EPR studies in the one dimensional [Cu(H_2O)(HTae)(4,4´-Bpy)](NO_3), the presence of long-range magnetic interactions appears to be the most plausible among all phenomena that could lead to a rhombic signal with collapsed hyperfine structure. The magnetic exchange pathways in [Cu(H_2O)(HTae)(4,4´-Bpy)](NO_3) were mainly related with hydrogen bonding magnetic exchange pathways between the copper atoms through the nitrate and water molecules located between adjacent [Cu(H_2O)(HTae)(4,4´-Bpy)](NO_3) metal organic chains ($J1_{dCu\cdots Cu}$ =7.00 Å; $J2_{dCu\cdots Cu}$ =7.35 Å) The magnetic exchange through the Bpy molecules (11 Å) is too long to be effective in this compound. [30]

In comparison, the absence of Cu(II) molecular signal in the Q-band EPR spectra of Closed·5H_2O indicates that the magnetic interactions between the copper centres are stronger than the magnetic coupling in [Cu(H_2O)(HTae)(4,4´-Bpy)](NO_3). The sharp and intense signal centred at about 11800 Gauss suggests the existence of a one-dimensional coupled system. If the crystal structure of the closed form is taken into account, three possible exchange pathways can be described: i) Cu-Bpa-Cu (dCu···Cu= 13.19 Å) and ii) Cu-Tae-Cu bridges (dCu···Cu= 8.05 Å) within the *"ths"* nets, and iii) magnetic coupling between copper cations of adjacent interpenetrated *"ths"* nets connected through hydrogen bonded nitrate and water molecules (dCu···Cu= 6.63 Å).

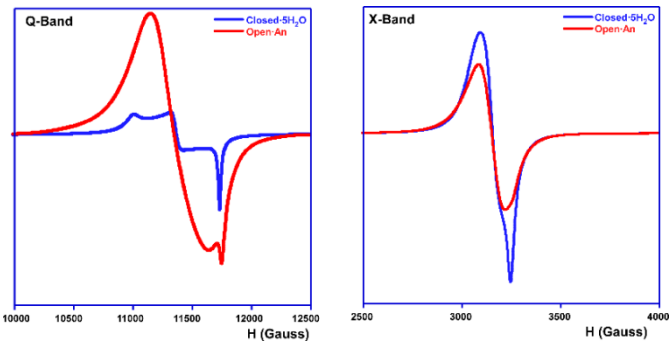

Fig. 6. EPR Q-Band and X-Band spectra of Closed·5H_2O and thermally activated open-anhydrous compounds.

Comparing the Cu···Cu distance values of [Cu(H_2O)(HTae)(4,4´-Bpy)](NO_3) and Closed·5H_2O compounds, and considering also that the magnetic exchange is stronger in Closed·5H_2O than in [Cu(H_2O)(HTae)(4,4´-Bpy)](NO_3), the most plausible scenario is that the magnetic exchange occurs more efficiently across the Cu atoms linked through the Tae ligand. Despite the Cu···Cu distance is longer (dCu···Cu= 8.05 Å) in Closed·5H_2O than the shortest one observed for copper atoms in [Cu(H_2O)(HTae)(4,4´-Bpy)](NO_3) (dCu···Cu= 7.00 Å), the magnetic coupling across covalently bonded atoms in Closed·5H_2O is more effective than through hydrogen bonded guest molecules in [Cu(H_2O)(HTae)(4,4´-Bpy)](NO_3).

The similarities between the EPR spectra of Closed·5H_2O and Open·2.4H_2O compounds discard an effective magnetic exchange through the solvent molecules, because, more probably, the guess species location and hydrogen bond bridges are different in the Open and Closed forms of the studied compounds, and hence, differences in their EPR spectra would be expected.

The thermal induced closed to open transformation causes a loss of long-range order in the crystal structure of Open·An compound that is reflected in its EPR spectra. Both for Q and X band quasi-isotropic EPR spectra, result of the signal broadening due to the disorder during the thermal activation, are observed.

Magnetic Properties

Is has not been possible to carry out the susceptibility measurements of Closed·$5H_2O$ because the high-vacuum conditions used in the experiments induces the dehydration of the sample, and the stabilization of the Open·An form. Magnetic measurements were performed on powdered Open·An sample from room temperature to 5K at a magnetic field of 0.1T. The thermal evolution of the χ_m and χ_mT product for the open form is shown in Fig. S8.

While the magnetic susceptibility increases from 300K to 5K, a weak decrease for the χ_mT product curve is observed below the Curie temperature, indicative of a weak antiferromagnetic coupling of the metal centres at low temperatures. This interpretation was confirmed by the slightly negative Weiss temperature, θ= -0.15K, obtained from the fit of the Curie-Weiss plot. The Curie constant obtained from the susceptibility fitting, 0.454 emuKmol$^{-1,}$ is near the expected value for a magnetically isolated Cu^{2+} (S=1/2 with g>2) cation.

Taking into account the crystal structure, magnetic coupling between the copper cations has to be very weak, and near the ideal paramagnetic behaviour observed in the experimental data, in good agreement with the magnetic coupling of copper cations through Tae ligands observed by EPR spectroscopy.

BET surface area and High Pressure adsorption

N_2 and high pressure CO_2 and CH_4 sorption experiments involve an initial thermal activation stage of the samples. Therefore, and taking into account the information obtained in the thermal properties section, the Open·An form of the studied compounds is always stabilized before the gas sorption experiments.

Nitrogen sorption at 77K reveals a mixture of type I and II isotherms. The type I isotherm can explain the first adsorption step ascribed to the micro-porosity of the material, BET= 3.8 m^2/gr (Fig. S9), whilst the second increase at relative pressures near 1 is related with a multilayer sorption process at the surface of the coordination polymer crystals. Despite the low surface area of the material, the high-pressure CO_2 and CH_4 adsorption can trigger the accommodation of gas molecules within the flexible interpenetrated structure. [31] Fig. 7 shows the pure-component absolute sorption isotherms for CH_4 (0-100 bar), and CO_2 (0-50 bar) at 0, 15, 30 and 45ºC. A mixture between type I and type II isotherms ascribed to the micro-porous encapsulation of the gases within the interpenetrated metal organic nets, followed by a multilayer adsorption in the surface of the single crystals is observed. Some degree of irreversibility is observed in the sorption experiments, specifically for CO_2, in which the hysteresis between the adsorption and desorption curves is more evident.

In order to acquire information about the microporous nature of the material, as well as of the adsorbent-adsorbate interactions within the pores of the open crystal structure, the sorption isotherms at different temperatures were fitted with a single component Freundlich model in the low pressure region (0-20 atm), in which the surface adsorption is not predominant.

As expected from the obtained BET surface area, the CO_2 uptake is very limited, and even more limited is the CH_4 sorption. Compared with previously studied MOF materials, the adsorption capacity is very low, however, CO_2/CH_4 selectivity values as high as 25 at low-pressures and of 15 at intermediate pressures are observed (Fig. 7 (c)). If the qCO_2/qCH_4 ratios between the capacities obtained from the Freundlich fitting (Table 3) are plotted at different temperatures (Inset-Fig. 7 (c)), an increase of the selectivity for CO_2 is observed when increasing the temperature.

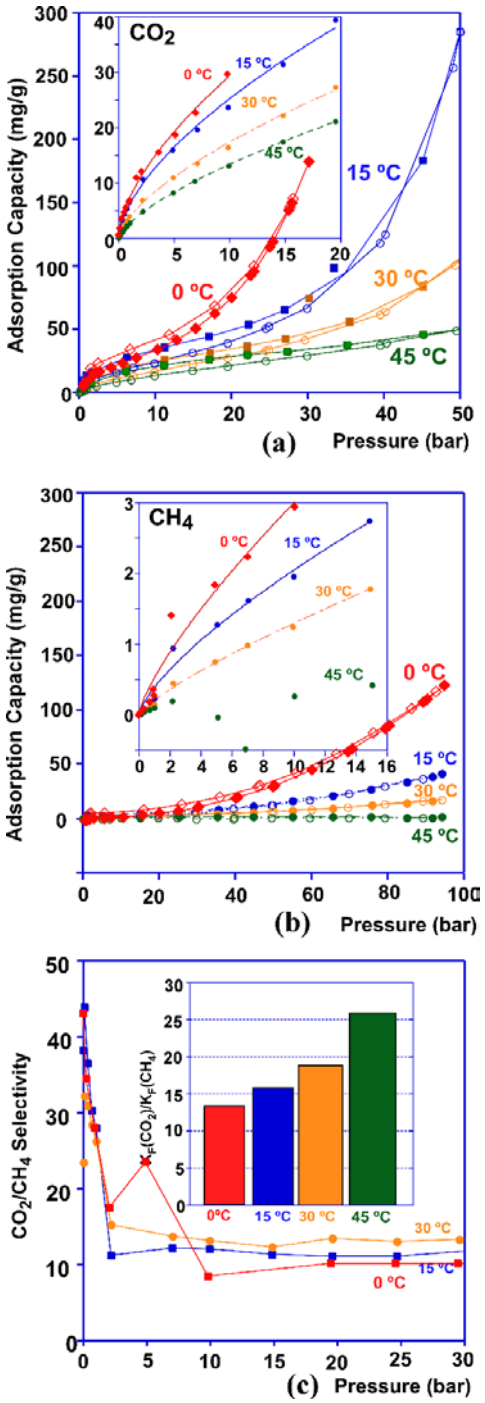

Fig.7. High Pressure (a) CO_2 and (b) CH_4 sorption (filled marks) and desorption (open marks) isotherms at 0, 15, 30 and 45ºC. (c) CO_2/CH_4 ratio between the equilibrium loadings of CO_2 and CH_4 adsorbed at different pressures. Inset: qCO_2/qCH_4 ratio for the adsorption capacities obtained based on the Freundlich fitting of the low-pressure data (0-20 bars).

Selectivity for CO_2/CH_4 equimolar mixture was calculated based on Ideal Adsorbed Solution Theory (IAST). The mixed-gas adsorption behaviour was extracted from the pure-component isotherms. Such estimations are essential in practice because collecting experimental data on mixture adsorption is time consuming and extremely rare. The obtained selectivity values are in good agreement with the experimental ones, with qCO_2/qCH_4 ratios of 25 and 15 at low and intermediate pressures, respectively (Fig. S10).

Table 3 Adsorption capacities (K_F (mg/g)) and adsorption constant (n) obtained for the fitting of the data with a Freundlich model.

CO_2	**0ºC**	**15ºC**	**30ºC**	**45ºC**
K_F (mg/g)	7.0(2)	6.1(3)	3.9(1)	2.78(3)
N	1.61(5)	0.614(5)	0.64(3)	0.68(1)
R	0.9974	0.9982	0.9993	0.9999
CH_4	**0ºC**	**15ºC**	**30ºC**	**45ºC**
K_F (mg/g)	0.52(9)	---	0.23(2)	0.107(6)
N	1.3(2)	0.75(7)	0.74(5)	0.82(1)
R	0.9811	0.9952	0.9977	0.9999

Isosteric heat for CO_2 and CH_4 was calculated interpolating the values of the equilibrium pressures at given equilibrium capacities at different temperatures (0, 15, 30 and 45ºC for CO_2 and 15, 30 and 45ºC for CH_4) (Fig. S10). For the CH_4 measurements, the adsorption isotherm at 45ºC was discarded for the isosteric heat calculations, due to the noise of the measurement ascribed to the low sorption capacity of the material. (Fig. 8)

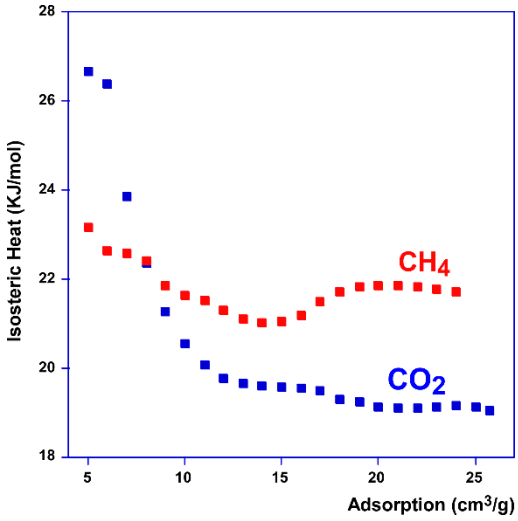

Fig.8. Isosteric heat of adsorption for CO_2 and CH_4 at different adsorption fillings.

Isosteric heat values for CO_2 near 32 KJ/mol are obtained at low filling rates. A decreasing evolution of the isosteric heat is observed with the pores filing down to 20 KJ/mol at 0.0008mol/g. With slightly lower isosteric heat values, the same tendency is observed for methane sorption.

In comparison with previously reported isosteric heat values for different metal organic frameworks, the values obtained for the studied compound are higher than the CO_2 isosteric heat for MOFs without open metal sites in their structures, such as ZIF family, [32] but lower than the values obtained for MOFs with strong interacting open metal sites, such as MOF74 materials. [33] Similar isosteric heat values have been reported for CO_2 sorption in HKUST-1, [34] a metal organic framework with exposed copper metal centres. [35]

Experimental

Materials and methods

Commercially available reagent grade chemicals were purchased from Sigma-Aldrich, and used without further purification: 1,2-Bis(4-pyridyl)ethane (Bpa), 1,1,2,2-tetraacetylethane (H_2Tae), $Cu(NO_3)_2{\cdot}H_2O$ and ethanol.

Synthesis

The single-crystals of the studied compound were crystallized from saturated ethanolic solutions.

Closed·5H_2O: 0.05 mmol of $Cu(NO_3)_2{\cdot}H_2O$ and 0.05 mmol of H_2Tae were dissolved in 12 mL of ethanol at 80ºC. After dissolving the H_2Tae ligand, the solution was slowly tempered at room temperature. Finally, 0.05 mmol of Bpa organic ligand was added carefully under stirring. After one week, plate shaped single-crystals began to crystallize. After the crystallization, the samples were washed with ethanol and dried at room temperature.

Open·2.4H_2O and Closed·3.6H_2O: Similar procedure was carried out, using double of Bpa concentration (0.1mmol) in this case. After one-week, a pale green polycrystalline powder (Open·2.4H_2O) with a minor amount of dark green single crystals (Closed·3.6H_2O) were obtained.

Open·An: The open anhydrous phase (Open-An) is obtained by thermal activation of Closed·5H_2O or Open·2.4H_2O compounds at 80ºC during 15 min. While the Closed·5H_2O → Open·An involves a sudden structural pores opening, the Open·2.4H_2O → Open·An thermal activation is a continuous process involving a progressive structural compression as a consequence of the continuous release of water molecules.

Single crystal X-ray diffraction

Single crystals of Closed·5H_2O and Closed·3.6H_2O were selected and mounted in a glass fibre. Firstly, a standard short program was used to obtain the crystal lattice and to confirm the quality of the crystals from a few diffraction images. Once the unit cells and the quality of the single-crystals were determined, the data collection of the complete Ewald sphere was carried out. Diffraction data were collected on an Agilent Supernova single source diffractometer with Mo Kα radiation at 100K. Data reduction was done with the CrysAlis RED program. [36] The diffraction data were corrected for Lorentz and polarization effects [37], as well as for the absorption, taking into account the crystal shape and size. The structure was solved by direct methods (SIR-2011 [38]) and refined by the full-matrix least-squares procedure based on F^2, using the SHELXL 97 [39], a computer program belonging to the WINGX software package. [40] The scattering factors were taken from the International Tables for Crystallography. [41] Details of

crystal data, intensity collection, and some features of the structural refinement are reported in Table 1.

Table 1 Crystallographic data and structure refinement parameters for crystal data and structure refinement of Closed·$5H_2O$ and Closed·$3.6H_2O$ crystal structures.

Compound	**Closed·$5H_2O$**	**Closed·$3.6H_2O$**
Formula	$C_{136}H_{144}Cu_8N_{24}O_{60}$	$C_{136}H_{144}Cu_8N_{24}O_{54.40}$
Fw (g/mol)	3583.07	3493.55
Crystal System	Orthorhombic	Orthorhombic
Colour	Green	Green
Space Group, N^{er}	*Fddd*, 70	*Fddd*, 70
a(Å), b(Å), c(Å)	10.9218(4) 23.5976(5) 34.2826(15)	11.1575(10) 23.7123(15) 33.583(3)
Z, F (000), T (K)	2, 3680, 100(2)	2, 3590.4, 100(2)
$\mu(mm^{-1})$	1.03	1.02
$\rho_{Calc.}$(g/cc)	1.347	1.306
Crystal Size (mm)	0.20× 0.20 × 0.04	0.16 × 0.13 × 0.04
Radiation (λ(Å))	0.71073	0.71073
N^{er} of reflns,	2544	2350
Reflns. (I>2σ(I))	1729	1721
h,k,l intervals	-12≥h≥14, -29≥k≥31, -45≥l≥43	-14≥h≥12, -29≥k≥29, -42≥l≥40
R(int), R(sigma)	0.068, 0.049	0.058, 0.063
R1, wR2(obs) (I>2σ(I))	0.0951, 0.2491	0.116, 0.289
R1, wR2(all)	0.133, 0.274	0.147, 0.310
GooF S	1.09	1.12
N^{er} of par./res.	141/9	131/6
L. Diff. Peak (e.Å^{-3})	1.54	1.659
L. Diff. Hole (e.Å^{-3})	0.97	-0.954

An initial analysis of the reciprocal space revealed similar unit cells for Closed·$5H_2O$ and Closed·$3.6H_2O$ single crystals. The crystal structures were solved by direct methods in the *Fddd* (70) space group. One copper atom lying on a special position, and the nitrogen, oxygen and carbon atoms belonging to the Bpa and Tae ligands were located for both structures.

For Closed·$5H_2O$, two disordered nitrate groups, the first semi-coordinated to the copper cations and the second type located in the pores of the crystal structure were located in successive refining cycles. Applying the charge neutrality principle to the initial structural model, the sum of the occupation factors of disordered nitrate molecules was restricted to 0.25. The crystal structure refinement of Closed·$3.6H_2O$ reveals only one crystallographic independent nitrate group (0.5 occupation factor) semi-coordinated to the copper cation. Both for Closed·$3.6H_2O$ and Closed·$5H_2O$ structures, the nitrate groups were refined with isotropic thermal displacements, and the N-O and O-O bond distances were restricted to 1.25(1) Å and 2.15(1) Å. Finally, 5 and 3.6 disordered crystallization water molecules were located and refined with isotropic thermal parameters within the pores of Closed·$3.6H_2O$ and Closed·$5H_2O$ frameworks, respectively. Occupation factors for water molecules were manually estimated until similar thermal displacements were obtained. The hydrogen atoms belonging to the Bpa and Tae organic molecules were fixed geometrically, allowing them to ride on their parent carbon atoms, C-H 0.93 Å; $U_{Iso}(H)= 1.2U_{eq}(C)$ Å^2 for the hydrogen atoms belonging to the pyridyl groups of the Bpa, and C-H 0.96 Å; $U_{Iso}(H)= 1.2U_{eq}(C)$ (Å^2) for the methyl groups of the HTae ligand. The hydrogen atoms of the water molecules were not located in the Fourier density map. The simplifications of the crystal structures and topological studies were carried out with TOPOS Pro [42] and PLATON [43] softwares.

Powder X-ray diffraction

The synthesized samples were characterized by powder X-ray diffraction. The data were recorded in a Bruker D8 Advance Vário diffractometer (Cu$K\alpha_1$ radiation), 2ϑ range= 5-70 º, step size= 0.015 º, exposure time = 10s per step at room temperature. Pattern Matching refinements analyses were carried out with Fullprof Suite software package (Fig. S11). [44] Because of the similarities between the structural models of Closed·$3.6H_2O$ and Closed·$5H_2O$ compounds is difficult to distinguish between both phases by powder x-ray diffraction. All attempts to get a reasonable Rietveld refinement with both structural models give rise to a poor fitting of the patterns because of the preferred orientation of the samples derived from the plate like morphology of the single crystals. Due to the similarities in the cell parameters of both phases, the pattern matching analysis does not allow obtaining reliable information to discern if both phases are present in the samples obtained at different synthetic conditions. Nevertheless, the thermal analyses confirms that all the samples synthesized in the conditions reported for Closed·$5H_2O$ possess an initial weight loss that agrees with the existence of five water molecules instead of the 3.6 H_2O reported for Closed·$3.6H_2O$.

All attempts to determine the crystal structure of Open·$2.4H_2O$ from powder diffraction data were unsuccessful. During the indexing process, a rhombic cell similar to that of the Closed compound was obtained, indicating that the Closed and open structures are nearly related. In order to corroborate this hypothesis, a pattern matching was carried out starting from the *Fddd* symmetry and the single crystal cell parameters of the Closed structure. The final fit is consistent with the rhombic cell and *Fddd* symmetry, despite some slight deviations discussed more profoundly in the Result and Discussion section.

Characterization

The percentages of the elements were calculated from C, N, H elemental analysis. Closed·$5H_2O$: Exp.: H 5.3(5) %, C 45.0(1) % and N 9.2(2) %, Theor.: H 5.19%, C 42.15 % and N 9.84 %. Open·$2.4H_2O$: Exp.: H 5.3(5) %, C 45.0(1) % and N 11.5(6) %, Theor.: H 4.84%, C 44.59 % and N 10.41 %**.** The experimental density of the crystals was not determined because the compound is dissolved in the high density solvents used in the density determination by flotation method.

The infrared spectra were recorded on a Jasco FT/IR-6100 spectrometer with pressed KBr pellets (400-4000 cm^{-1}). Solid diffuse reflectance spectrum was registered at room temperature on a Varian Cary 5000 spectrophotometer in the 50000-4000 cm^{-1} range.

Physical measurements

The temperature-dependent PXRD in air atmosphere were carried out on a Bruker D8 Advance Vantec diffractometer (Cu$K\alpha$ radiation), equipped with a variable-temperature stage HTK2000 Measurements were performed in the 30 to 500ºC temperature range, each 10ºC (2ϑ range= 9-30 º, step size= 0.01 º, exposure time = 0.5 s per step). The thermal evolution of the cell parameters and cell volume for the Open·2.4H_2O structure were obtained performing a peak fit of the (004), (040) and (113) reflections. Thermal analyses were carried out in air atmosphere, up to 500ºC, with a heating rate of 5ºCmin^{-1} on a Netzsch Sta Simultaneous DSC-TGA. EPR powder spectra were recorded on a Bruker ESP300 spectrometer (X- and Q-bands) equipped with Oxford low-temperature devices (magnetic field calibration: NMR probe; determination of the frequency inside the cavity: Hewlett-Packard 5352B microwave frequency counter). X and Q band EPR measurements were carried out on powdered samples of Closed·5H_2O, Open·2.4H_2O and Open·An compounds at several temperatures in the range 5-300 K. The spin Hamiltonian parameters for all the samples were estimated by comparison of the experimental spectra with those obtained by a computer simulation program working at the second order of the perturbation theory. The parameters were then optimized by the trial and error method. The magnetic measurements were performed on a Quantum Design MPMS-7 SQUID magnetometer in the temperature range 5–300 K. The magnetic field was 0.1 T, a value in the range of linear dependence of magnetization vs. magnetic field; even at 5.0 K. Surface area for Open·An was determined by nitrogen physisorption method on a Micrometrics ASAP 2010 instrument. High-pressure gas adsorption experiments were carried out in an iSorb HP1 (Quantachrome Instruments) high-pressure gas sorption analyser. All the samples used in gas sorption experiments were activated at 80ºC under vacuum during one day. Ideal selectivity gives an idea about the gas separation performance of a material. However, gases exist as mixtures in reality; therefore, it is better to report mixture selectivities of materials. Measuring single-component gas adsorption isotherms of materials is possible by using some commercial instruments; however, a similar type of measurements becomes very complex, expensive, and time consuming for gas mixtures. In this sense, IAST calculations are performed by pyIAST [45]. This method was used to calculate CO_2/CH_4 selectivity factors at 298 K based on single-component CO_2 and CH_4 isotherms and a theoretical gas mixtures of 15 mol percent CO_2 and 85 mol percent CH_4. Before the IAST calculations isotherms curves were fitted by interpolation of individual sorption points with pyIAST, and in a second step the selectivity factors were calculated.

Conclusions

Solvent and nitrate anion location within the $[Cu_2(Tae)(Bpa)_2]^+$ cationic interpenetrated networks plays a crucial role in the stabilization of the different closed or open forms of the $[Cu_2(Tae)(Bpa)_2](NO_3)_2{\cdot}nH_2O$ crystal structure. Even if the crystal framework is approximately the same for all the phases, the position of the solvent molecules and their interaction with the crystal framework takes a crucial role triggering the closed to open structural transformation. The random disorder of the nitrate groups, added to the existence of one nitrate per copper atom, allows the existence of at least one open metal site per copper atoms in the structure. Because of the thermal activation of the samples, a reduction of the crystallinity is observed due to the loss of long-range order in the crystal structures. The rearrangement of the interpenetrated nets jointly with the stretching of helical metal organic chains within the *"ths"* nets, are the main mechanisms explaining the structural breathing.

Magnetic behaviour and EPR spectroscopy studies reveal that the Cu-Tae-Cu bridges are the most effective magnetic exchange pathways, discarding any magnetic exchange through the solvent molecules trapping between the interpenetrated nets.

Despite the porosity of the interpenetrated framework is very low, the high-pressure incorporation of CO_2 and CH_4 within the crystal structure is possible. The open form material exhibits good CO_2/CH_4 selectivity, but low gas uptake, even near zero for CH_4 at 45ºC. The uptake reduction of CH_4 with the increase of temperature is more acute than for CO_2, a fact that enhances the CO_2/CH_4 selectivity with the increase of temperature. This is clearly related with the stronger host-CO_2 interactions in comparison with the host-CH_4 ones. Isosteric heat calculations support the affinity of the studied materials for CO_2 uptake at low gas loadings. Once the preferential adsorption sites are occupied, the isosteric heat of adsorption for CO_2 decrease more abruptly than this one for CH_4.

Conflicts of interest

There are no conflicts to declare.

Acknowledgements

This work has been financially supported by the "Ministerio de Economía y Competitividad" (MAT2016-76739-R (AEI/FEDER, EU), the "Gobierno Vasco" (Basque University Research System Group, IT-630-13 and Economic Development and Competitiveness, ACTIMAT (KK-2015/00094) and LISOL (KK-2016/00095) projects, ELKARTEK program) which we gratefully acknowledge. Joseba Orive wishes to thank CONICYT for the 2015 FONDECYT postdoctoral project (N^{er} 3150455). The authors thank the technicians of SGIker (UPV/EHU).

Notes and references

1 (a) H. Furukawa, K. E.Cordova, M. O'Keeffe, O. M. Yaghi**,** *Science*, 2013, **341**, 1230444. (b) O. M. Yaghi, M. O'Keeffe, N. W. Ockwig, H. K. Chae, M. Eddaoudi, J. Kim, *Nature,* 2003, **423**, 705.

2 (a) W. M. Bloch, N. R. Champness, C. J. Doonan, *Angew. Chem. Int. Ed.* 2015, **54**, 12860–12867, (b) N. C. Burtch, H. Jasuja, K. S. Walton, *Chem. Rev.*, 2014, **114**, 10575–10612, (c) Y. Cui, B. Li, H. He, W. Zhou, B. Chen, G. Qian, *Acc. of Chem. Res.*, 2016, **49**, 483–493, (d) R. Fernández Luis, J. Orive, E. S. Larrea, M. K. Urtiaga, M. I. Arriortua, *CrystEngComm*, 2014, **16**, 10332–10366, (e) T. Devic, C. Serre, *Chem. Soc. Rev.*, 2014, **43**, 6097–6115, (f) C. I. Ezugwu, N. A. Kabir, M. Yusubov, F. Verpoort, *Coor. Chem. Rev.* 2016, **307***, Part 2*, 188–210.

3 K. Vasanth, K. Preuss, M.-M. Titirici, F. Rodríguez-Reinoso, *Chem. Rev.* 2017, **117**, 1796−1825.

4 (a) E. Coronado, G. Minguez Espallargas, *Chem. Soc. Rev.*, 2013, **42**, 1525-1539, (b) T. Grancha, M. Mon, F. Lloret, J. Ferrando-Soria, Y. Journaux, J. Pasán, E. Pardo, *Inorg. Chem.*, 2015, **54**, 8890–8892, (c) R. Fernández de Luis, M. K. Urtiaga, J. L. Mesa, K. Vidal, L. Lezama, T. Rojo, M. I. Arriortua, *Chem. Mater.*, 2010, **22**, 5543–5553, (d) E. S. Larrea, J. L. Mesa, J. L. Pizarro, R. Fernández de Luis, J. R. Fernández, T. Rojo, M. I. Arriortua, *Dalton Trans.*, 2012, **41**, 14170–14179.

5 (a) Z. Hu, B. J. Deibert, J. Li, *Chem. Soc. Rev.*, 2014, **43**, 5815–5840, (b) L. E. Kreno, K. Leong, O. Farha, M. Allendorf, R. P. Van Duyne, J. T. Hupp, *Chem. Rev.*, 2012, **112**, 1105–1125, (c) A. Calderón-Casado, G. Barandika, B. Bazán, M. K. Urtiaga, M. I. Arriortua, *CrystEngComm*, 2013, **15**, 5134-5137. (d) S. L. Jackson, A. Rananaware, C. Rix, S. V. Bhosale, K. Latham, *Cryst. Growth Des.*, 2016, **16**, 3067–3071.

6 (a) G. Férey, *Dalton Trans.*, 2016, **45**, 4073–4089, (b) Z.-J. Lin, J. Lü, M. Hong, R. Cao, *Chem. Soc. Rev.*, 2014, **43**, 5867–5895, (c) A. Calderón-Casado, G. Barandika, B. Bazán, M. K. Urtiaga, O. Vallcorba, J. Rius, M. I. Arriortua, *CrystEngComm*, 2011, **13**, 6831–6838, (d) A. Fidalgo-Marijuan, G. Barandika, B. Bazán, M. K. Urtiaga, M. I. Arriortua, *CrystEngComm*, 2013, **15**, 4181–4188, (e) F. Llano-Tomé, B. Bazán, M. K. Urtiaga, G. Barandika, A. Fidalgo-Marijuan, R. Fernández de Luis, M. I. Arriortua, *CrystEngComm*, 2015, **17**, 6346–6354.

7 (a) S. Horike, D. Umeyama, S. Kitagawa, *Acc. of Chem. Res.*, 2013, **46**, 2376–2384, (b) P. Ramaswamy, N. E. Wong, G. K. Shimizu, *Chem. Soc. Rev.*, **2014**, *43*, 5913–5932, (c) R. Fernández de Luis, A. Ponrouch, R. Palacín, M. K. Karmele Urtiaga, M. I. Arriortua, *J. Solid State Chem.*, 2014, **212**, 92–98.

8 Z. Hasan, S. H. Jhung, *J. Hazar. Mat.*, *283*, **2015**, 329-339.

9 (a) A. Dhakshinamoorthy, M. Opanasenko, J. Čejka, H. Garcia, *Adv. Synth. Catal.* 2013, **355**, 247-268; (b) A. Dhakshinamoorthy, A. M. Asiri, H. Garcia, *Chem. Eur. J.* 2016, **22**, 8012-8024, (c) A. Dhakshinamoorthy, A. M. Asiri, H. Garcia, *Chem. Soc. Rev.* 2015, **44**, 1922-1947.

10 (a) T. Zhang, W. Lin, *Chem. Soc. Rev.,* 2014, **43**, 5982-5993; (b) Z. Xie, W. Xu, X. Cui, Y. Wang, *ChemSusChem,* 2017, **10**, 1645 –1663, (c) R. Kaur, K.-H. Kim, A. K. Paul, A. Deep, *J. Mater. Chem. A*, 2016, **4**, 3991-4002.

11 (a) H.-C. Zhou, S. Kitagawa, *Chem. Soc. Rev.*, 2014, **43**, 5415–5418, (b) E. Amayuelas, A. Fidalgo-Marijuan, G. Barandika, B. Bazán, M. K. Urtiaga, M. I. Arriortua, *CrystEngComm*, 2015, **17**, 3297–3304, (c) L. Bravo-García, G. Barandika, B. Bazán, M. K. Urtiaga, M. I. Arriortua, *Polyhedron*, 2015, **92**, 117–123, (d) A. Fidalgo-Marijuan, G. Barandika, B. Bazán, M. K. Urtiaga, L. Lezama, M. I. Arriortua, *Inorg. Chem.*, 2013, **52**, 8074–8081.

12 Q. Guo, C. Merkens, R. Si, U. Englert, *CrystEngComm*, 2015, **17**, 4383–4393.

13 (a) S. Dutta, P. Biswas, S. K. Dutta, K. Nag, *New J. Chem.*, 2009, **33**, 847–852, (b) M. Rancan, A. Dolmella, R. Seraglia, S. Orlandi, S. Quici, L. Sorace, L. Armelao, *Inorg. Chem.* 2012, **51**, 5409–5416.

14 (a) M. Rancan, J. Tessarolo, M. Casarin, P. L. Zanonato, S. Quici, L. Armelao, *Inorg. Chem.*, 2014**, 53**, 7276–7287, (b) M. Rancan, A. Dolmella, R. Seraglia, S. Orlandi, S. Quici, L. Armelao, *Chem. Commun.*, 2012, **48**, 3115–3117 (c) J. K. Cherutoi, J. U. Sandifer, U. R. Pokharel, F. R. Fronczek, S. Pakhomova, A. W. Maverick, *Inorg. Chem.*, 2015*,* **54**, 7791–7802, (d) T. Liu, Y. Liu, W. Xuan, Y. Cui, *Angew. Chem. Int. Ed.,* 2010, **49**, 4121–4124.

15 C. Pariya, F. R. Fronczek, A. W. Maverick, *Inorg. Chem.* 2011, **50**, 2748–2753.

16 (a) C. Tsiamis, A. G. Hatzidimitriou, L. C. Tzavellas, *Inorg. Chem.*, 1998, **37**, 2903–2909, (b) B. Chen, F. R. Fronczek; A. W. Maverick, *Acta. Crystallogr. C*, 2004, ***C60***, m147-m149 (c) G. Voutsas, L. C. Tzavellas, C., Tsiamis, *Struct. Chem.* 1999, **10**, 53-57, (c) B. Chen, F. R. Fronczek, A. W. Maverick, *Chem. Commun.* 2003, 2166-2167, (d) S. S. Turner, D. Collison, F. E. Mabbs, M. Halliwell, *J. Chem. Soc., Dalton Trans.*, 1997, 1117–1118 (e) J. Yoshida, S. Nishikiori, R. Kuroda, H. Yuge, *Chem. – A Eur. J.* 2013, **19**, 3451–3457, (f) H. Sakamoto, R. Matsuda, S. Bureekaew, D. Tanaka, S. Kitagawa, S. *Chem.– A Eur. J.* **2009**, *15*, 4985–4989.

17 (a) B. Chen, F. R. Fronczek, A. W. Maverick, *Inorg. Chem.*, 2004, **43**, 8209–8211, (b) B. Kilduff, D. Pogozhev, S. A Baudron, M. W. Hosseini, *Inorg. Chem.*, 2010, **49**, 11231–11239, (c) V. D. Vreshch, A. B. Lysenko, A. N. Chernega, J. A. K. Howard, H. Krautscheid, J. Sieler, K. V. Domasevitch, *Dalton Trans.,* 2004, 2899-2903, (d) M. Kondracka, U. Englert, U. *Inorg. Chem.* 2008, **47**, 10246–10257, (e) A. D. Burrows, K. Cassar, M. F. Mahon, J. E. Warren, *Dalton Trans.*, 2007, 2499–2509.

18 (a) A. D. Burrows, K. Cassar, M. F. Mahon, S. P. Rigby, J. E. Warren, *CrystEngComm*, 2008, **10**, 1474, (b) Q. Yang, X. Tan, S. Wang, J. Zhang, L. Chen, J.-P. Zhang, C.-Y. Su, *Micro. Meso. Mat.* 2014 **187**, 108–113.

19 (a) Y. Zhang, S. Wang, G. D. Enright, S. R. Breeze, *J. Am. Chem. Soc.* 1998, **120**, 9398-9399, (b) J. A. Tovilla, S. Hernández-Ortega, J. Valdés-Martínez, *Acta Crystallogr. E,* 2009, **65**, m366–m367, (c) J. B. Lambert, Z. Liu, *J. Chem. Crystallogr.* 2007, **37**, 629-639.

20 (a) R. Fernández de Luis, E. S. Larrea, J. Orive, L. Lezama, M. I. Arriortua, *Inorg. Chem.*, 2016, **55**, 11662–11675, (b) E. S. Larrea, R. Fernández de Luis, M. I. Arriortua, *Molecules,* 2016, **21**, 1651-1654.

21 B. S. Luisi, V. C. Kravtsov, B. D. Moulton, *Cryst. Growth & Des.*, 2006, **6**, 2207–2209

22 (a) L. Carlucci, G. Ciani, D. M. Proserpio, *Coord. Chem. Rev.*, 2003, **246**, 247−289, (b) Z. Zhang, J. Liu, Y. Li, S. Yao, E. Wang, X. Wang, *J. Solid State Chem.*, 2010, **183**, 228−233.

23 (a) H.-L. Jiang, T. A. Makal, H.-C. Zhou, *Coord. Chem. Rev.,* 2012, **257**, 2232–2249, (b) A. Ferguson, L. Liu, S. J. Tapperwijn, D. Perl, F.-X. Coudert, S. Van leuvenbergen, T. Verbiest, M. A. van der Veen, S. G. Telfer, *Nature Chem.,* 2016, **8**, 250–257.

24 (a) L.-H. Xie, M. P. Suh, *Chem. Eur. J.,* 2011, **17**, 13653-13656, (b) K. L. Mulfort, O. K. Farha, C. D. Malliakas, M. G. Kanatzidis, J. T. Hupp, *Chem. Eur. J.,* 2010, **16**, 276-281.

25 S. Noro, *Phys. Chem. Chem. Phys.*, 2010, **12**, 2519-2531.

26 M. Llunell, D. Casanova, J. Cirera, P. Alemany, S. Alvarez, *Shape: Program for the Stereochemical Analysis of Molecular Fragments by Means of Continuous Shape Measures and Associated Tools*, Departament de Química Física, Departament de Química Inorgànica, and Institut de Química Teòrica i Computacional - Universitat de Barcelona, Barcelona, **2013**.

27 (a) I. D. Brown, *Structure and Bonding in Crystals* (Eds.: M.O'Keeffe, A. Navrotsky), vol. 2, Academic Press, New York, **1981,** (b) N. S. Brese, M. O´Keeffe, M., *Acta. Crystallogr.*, 1991, **B47**, 192-197, (c) I. D. Bronw, D. Altermat, *Acta. Crystallogr.*, 1985, **B41**, 244-247.

28 (a) A. L. Goodwin, M. Calleja, M. J. Conterio, M. T. Dove, J. S. O. Evans, D. A. Keen´, L. Peters, M. G. Tucker, *Science,* **2008**, *319*, 794-797, (b) I. Grobler, V. J. Smith, P. M. Bhatt, S. A. Herbert, L. J. Barbour, *J. Am. Chem. Soc.*, 2013, **135**, 6411–6414.

29 (a) C. Serre, F. Millange, C. Thouvenot, M. Noguès, G. Marsolier, D. Louër, G. Férey, *J. Am. Chem. Soc.*, 2002, **124***,* 13519–13526, (b) S. Bourrelly, P. L. Llewellyn, C. Serre, C. Millange, G. Férey, *J. Am. Chem. Soc.*, 2005, **127**, 13519–13521, (c) A. Loiseau, C. Serre, C. Huguenard, G. Fink, F. Taulelle, M. Henry, T. Bataille, G. Férey, *Chem. Eur. J.,* 2004, **10**, 1373-1382.

30 a) R. Cortés, L. Lezama, J. I. R. Larramendi, M. Insausti, J. V. Folgado, G. Madariaga, T. Rojo, *J. Chem. Soc., Dalton Trans.,* 1994, 2573-2579, (b) A. B. Caballero, A. Rodríguez-Diéguez, L. Lezama, E. Barea, J. M. Salas, *Dalton Trans.,* 2011, **40**, 5180-5187.

31 Q. Yao, J. Su, O. Cheung, Q. Liu, N. Hedin, X. Zou, *J.Mater.Chem.*, 2012, **22**, 10345-51.

32 (a) J.-R. Li, Y. Mab, M. C. McCarthyb, J. Sculleya, J. Yub, H.-K. Jeong, P.-B. Balbuena, H.-C. Zhoua, *Coor. Chem. Rev.,* 2011, **255**, 1791–1823, (b) A. Phan, C. J. Doonan, F. J. Uribe-Romo, C. B. Knobler, M. O´Keeffe, O. M. Yaghi, *Acc. Chem. Res.* 2010, **43,** 58-67.

33 (a) Z. R. Herm, R. Krishna, J. R. Long, *Micro. Meso. Mater.,* 2012, **151**, 481–487, b) X. Wua, Z. Bao, B. Yuan, J. Wang, Y. Sun, H. Luo, S. Deng, *Micro. Meso. Mater.,* 2013*,* **180***,* 114–122.

34 (a) J. A. Mason, M. Veenstrab, J. R. Long, *Chem. Sci.* 2014, **5**, 32-51, (b) J. Moellmer, A. Moeller, F. Dreisbach, R. Glaeser, R. Staudt, *Micro. Meso. Mater.,* 2011, **138**, 140–148.

35 K. V. Kumar, K. Preuss, M.-M. Titirici, F. Rodríguez-Reinoso, *Chem. Rev.,* 2017, **117**, 1796−1825.

36 CrysAlis RED, version 1.171.33.55; *Oxford Diffraction*: Wroclaw, Poland, **2010**.

37 W. Yinghua, *J. Appl. Crystallogr.,* 1987, **20**, 258–259.

38 A. Altomare, G. Cascarano, C. Giacovazzo, A. Guagliardi, *J. Appl. Crystallogr.,* 1993, **26**, 343-350.

39 SHELX97, *Programs for Crystal Structure Analysis*. G. M. Sheldrick, Institüt für Anorganische Chemie der Universität, Tammanstrasse 4, D-3400 Göttingen, Germany, **1998**.

40 L. J. Farrugia, *J. Appl. Crystallogr.,* 1999, **32**, 837–838.

41 T. Han, *International Tables for X-ray Crystallography*, Kynoch Press, Birmingham, UK, 1973, vol. 4.

42 TOPOS 4.0, *A program package for multipurpose geometrical and topological analysis of crystal structures*, http://www.topos.ssu.samara.ru, 2012, (b) V. A. Blatov, A. P. Shevchenko, V. N. Serezhkin, *Acta Crystallogr.*, 1995, **A51**, 909-916, (c) I. A. Baburin, V. A. Blatov, *Acta Crystallogr.*, 2004, **B60**, 447-452, (d) E. V. Peresypkina, V. A. Blatov, *Acta Crystallogr.*, 2000, **B56**, 1035-1045, (e) V. A. Blatov, A. P. Shevchenko, *Acta Crystallogr.*, 2003, **A59**, 34-44.

43 PLATON, *A Multipurpose Crystallographic Tool*, Utrecht University, Utrecht, The Netherlands, Spek, A. L. **1998**.

44 J. Rodríguez-Carvajal, *J. Phys. B,* 1993, **192**, 55-69.

45 C. M. Simon, B. Smit, M. Haranczyk, *Pyiast: Ideal Adsorbed Solution Theory (IAST) Python Package. Comput. Phys. Commun.* 2016, **200**, 364−380.